Data Paper

The International Journal of Robotics Research
2024, Vol. 0(0) 1–14

DOI: 10.1177/02783649241230640
journals.sagepub.com/home/ijr


UTIL: An ultra-wideband time-difference-of-arrival indoor localization dataset

Wenda Zhao[1], Abhishek Goudar[1], Xinyuan Qiao[1] and Angela P. Schoellig[1,2]

Abstract

Ultra-wideband (UWB) time-difference-of-arrival (TDOA)-based localization has emerged as a promising, low-cost, and scalable indoor localization solution, which is especially suited for multi-robot applications. However, there is a lack of public datasets to study and benchmark UWB TDOA positioning technology in cluttered indoor environments. We fill in this gap by presenting a comprehensive dataset using Decawave's DWM1000 UWB modules. To characterize the UWB TDOA measurement performance under various line-of-sight (LOS) and non-line-of-sight (NLOS) conditions, we collected signal-to-noise ratio (SNR), power difference values, and raw UWB TDOA measurements during the identification experiments. We also conducted a cumulative total of around 150 min of real-world flight experiments on a customized quadrotor platform to benchmark the UWB TDOA localization performance for mobile robots. The quadrotor was commanded to fly with an average speed of 0.45 m/s in both obstacle-free and cluttered environments using four different UWB anchor constellations. Raw sensor data including UWB TDOA, inertial measurement unit (IMU), optical flow, time-of-flight (ToF) laser altitude, and millimeter-accurate ground truth robot poses were collected during the flights. The dataset and development kit are available at https://utiasdsl.github.io/util-uwb-dataset/.

Keywords

Ultra-wideband, time-difference-of-arrival, indoor localization

1. Introduction

Accurate and reliable indoor localization is a crucial enabling technology for many robotics applications, ranging from warehouse management to monitoring tasks. Over the last decade, ultra-wideband (UWB) radio technology has been shown to provide high-accuracy and obstacle-penetrating time-of-arrival (TOA) measurements that are robust to radio-frequency interference (Zafari et al., 2019). UWB chips have been integrated in the latest generations of consumer electronics including smartphones and smartwatches to support spatially aware interactions (Apple, 2022; Qorvo, 2022; Robert Triggs, 2022). During the FIFA World Cup 2022, UWB localization technology was used, for the first time, in an official football tournament to enhance the Video Assistant Referee (VAR) system by providing reliable, low-latency, and decimeter-level accurate ball tracking information (Adidas, 2022; Dowsett, 2022; KINEXON, 2022).

Similar to the Global Positioning System (GPS) (Enge, 1994), an UWB-based positioning system requires UWB radios (also called anchors) to be pre-installed in the environment as a constellation with known positions, which in turn serve as landmarks for positioning. In robotics (Nguyen et al., 2021a; Pfeiffer et al., 2021), the two common ranging schemes used for UWB localization are *(i)* two-way ranging (TWR) and *(ii)* time-difference-of-arrival (TDOA). In TWR, the UWB module mounted on the robot (also called tag) communicates with an anchor and acquires range measurements through two-way communication. In TDOA, UWB tags compute the difference between the arrival times of the radio packets from two anchors as TDOA measurements. Compared with TWR, TDOA does not require active two-way communication between an anchor and a tag, thus enabling localization of a theoretically unlimited number of devices (Hamer and D'Andrea, 2018). However, UWB TDOA-based localization systems still encounter difficulties in cluttered indoor environments (see Figure 1). Delayed and degraded radio signals caused by non-line-of-sight (NLOS) and multi-path radio propagation can greatly deteriorate positioning accuracy. In order to achieve reliable

[1]The University of Toronto Robotics Institute, Vector Institute for Artificial Intelligence, University of Toronto Institute for Aerospace Studies (UTIAS), Toronto, ON, Canada
[2]Munich Institute for Robotics and Machine Intelligence (MIRMI), Technical University of Munich, Munich, Germany

Corresponding author:
Wenda Zhao, Institute for Aerospace Studies, University of Toronto, 4925 Dufferin St., North York, Toronto, ON M3H 5T6, Canada.
Email: wenda.zhao@robotics.utias.utoronto.ca

UWB TDOA-based positioning in complex indoor environments, novel estimation algorithms are required to improve localization accuracy and robustness.

To foster research in this domain, this paper presents a comprehensive UWB TDOA dataset collected in a variety of cluttered indoor environments, including different types of static and dynamic obstacles. Low-cost DWM1000 UWB modules (Decaware, 2016) were used to construct cost-efficient indoor positioning systems for data collection. The dataset includes two parts: *(i)* an UWB TDOA identification dataset and *(ii)* a flight dataset. The goal of the identification dataset is to characterize the UWB TDOA measurement performance in line-of-sight (LOS) and non-line-of-sight (NLOS) conditions. It includes low-level UWB signal information such as signal-to-noise ratio (SNR) and power difference values. To create the NLOS scenarios, obstacles made of different materials commonly found in indoor settings were used, including cardboard, metal, wood, plastic, and foam. In the flight dataset, we conducted a cumulative total of roughly 150 min of real-world flights with a customized quadrotor and collected a comprehensive multimodal dataset to benchmark UWB TDOA localization performance for three-dimensional robot pose estimation. The quadrotor was commanded to fly with an average speed of 0.45 m/s in both obstacle-free and cluttered indoor environments with static and dynamic obstacles using four different anchor constellations. Raw sensor data including UWB TDOA, inertial measurement unit (IMU), optical flow, time-of-flight (ToF) laser altitude, and millimeter-accurate ground truth robot pose data from a motion capture system were collected during the flights.

The intended users of this dataset are researchers who are interested in UWB TDOA-based localization technology. The dataset can be used to model UWB TDOA measurement errors under various LOS and NLOS conditions. Also, users can study the UWB TDOA-based positioning performance *(i)* under different UWB anchor constellations, *(ii)* with and without obstacles, and *(iii)* using the centralized and decentralized TDOA mode (introduced in Section 3). Further, the users of this dataset are encouraged to design novel and practical estimation algorithms to enhance the accuracy and robustness of UWB TDOA-based positioning in cluttered indoor environments.

The main contributions of this dataset are as follows:

- An identification dataset for UWB TDOA measurements in a variety of LOS and NLOS scenarios involving obstacles of different materials, including cardboard, metal, wood, plastic, and foam.
- A comprehensive multimodal dataset from roughly 150 min of real-world flights in both obstacle-free and cluttered indoor environments, featuring both static and dynamic obstacles. We collected centralized and decentralized UWB TDOA measurements using four different anchor constellations.

2. Related work

Many public UWB datasets have been produced in literature for a variety of applications, including UWB radar (Ahmed et al., 2021; Brishtel et al., 2023; Ge et al., 2023; Zhang et al., 2023; Zhengliang et al., 2021), human motion tracking (Bocus and Piechocki, 2022; Delamare et al., 2020; Vleugels et al., 2021), and localization for mobile robots (Morón et al., 2023; Nguyen et al., 2021b; Queralta et al., 2020; Raza et al., 2019). In addition to these specific dataset papers, several UWB datasets have been publicly released as companions to research papers (Bregar and Mohorčič, 2018; Barral et al., 2019a; Ledergerber and D'Andrea, 2019; Pfeiffer et al., 2021). Considering the large amount

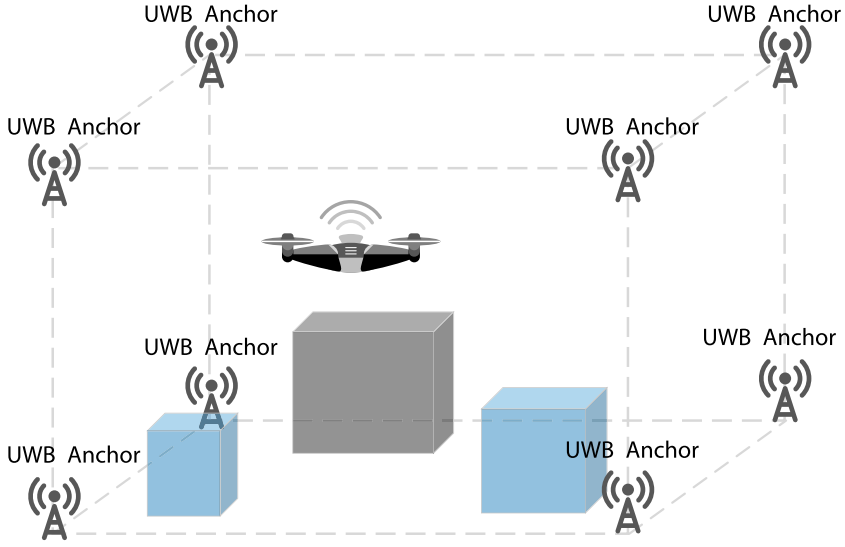

Figure 1. An UWB TDOA localization system in an indoor environment cluttered with wooden (blue boxes) and metal (the gray box) obstacles. UWB anchors are pre-installed with known positions in the space. The quadrotor, equipped with an UWB tag, receives TDOA measurements from the anchors for localization.

Table 1. Public UWB dataset for mobile robot localization. The LOS/NLOS testing refers to experiments to identify and model UWB measurements under LOS/NLOS scenarios. Time Domain UWB modules are high-performance UWB radio sensors originally developed by Time Domain Corporation (TDSR, 2022). Time Domain UWB modules can provide more accurate two-way ranging measurements at a higher price compared to low-cost Decawave's DWM1000 modules.

Reference	UWB mode	LOS/NLOS testing	Anchor constellations	Static obstacle	Dynamic obstacle	Dimension	UWB module
Bregar and Mohorčič (2018)	TWR	✓	4	✓	✗	2D	DWM1000
Li et al. (2018)	TWR	✗	1	✗	✗	3D	Time Domain
Barral et al. (2019b)	TWR	✓	1	✓	✗	2D	DWM1000
Arjmandi et al. (2020)	TWR	✗	5	✗	✗	3D	Time Domain
Queralta et al. (2020)	TWR	✗	4	✗	✗	3D	DWM1001
Nguyen et al. (2021b)	TWR	✗	3	✗	✗	3D	Time Domain
Ledergerber and D'Andrea (2019)	TWR and CIR values	✓	4	Wood, metal, and fabric (chair)	✗	2D	DWM1000
Morón et al. (2023)	TWR	✓	3	✓	✗	3D	DWM1001
Fontaine et al. (2023)	TWR	✓	1	✓	✗	3D	DWM1000
Pfeiffer et al. (2021)	TWR TDOA	✗	1	✗	✗	3D	DWM1000
Raza et al. (2019)	TDOA	✗	1	✗	✗	2D	DWM1001
UTIL dataset (ours)	TDOA	✓	4	Plastic, wood, metal, cardboard, and foam	Metal	3D	DWM1000

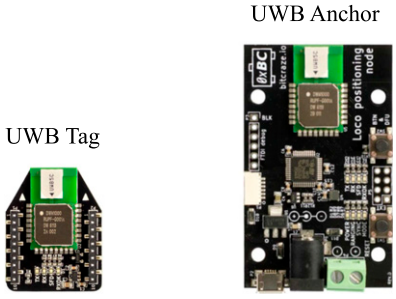

Figure 2. The Loco Positioning System anchor and tag from Bitcraze, based on Decawave's DWM1000 UWB modules, are used for the data collection.

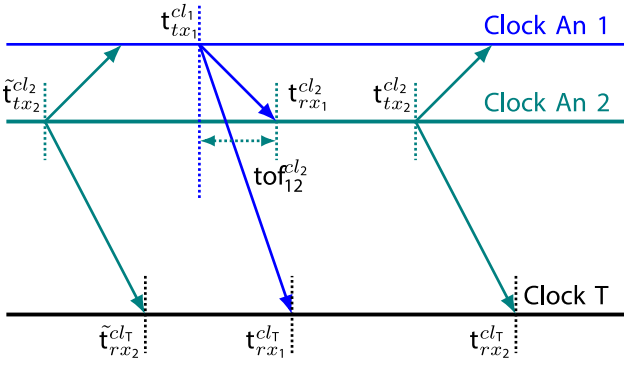

Figure 3. The sequence of UWB radio packets between the tag and anchor 1 and anchor 2. The clocks of anchor 1, anchor 2, and the tag are indicated as solid lines with different colors. The radio packets between the tag and anchors are denoted as solid arrow lines.

of applications of UWB technology, we focus on UWB-based localization for mobile robots and summarize the related UWB datasets, to the best of our knowledge, in Table 1 for an overview.

From Table 1, we can observe that many of the public UWB datasets focus on UWB TWR-based localization (Arjmandi et al., 2020; Barral et al., 2019b; Bregar and Mohorčič, 2018; Li et al., 2018; Morón et al., 2023; Nguyen et al., 2021b). For UWB TDOA-based positioning, Raza et al. (Raza et al., 2019) provided a dataset to compare the performance of UWB TDOA and narrowband Bluetooth-based localization technologies. However, the dataset only contains UWB and Bluetooth radio measurements, lacking other sensing modalities. Additionally, the data collection occurred in a simple 2D setup without any obstacles. Pfeiffer et al. (Pfeiffer et al., 2021) released their dataset along with their research work including both UWB TWR and TDOA measurements collected from a Crazyflie 2.1 nano-quadrotor. However, the dataset was also created in an obstacle-free environment.

Realistic indoor environments often contain different types of obstacles that might interfere with UWB radio signals. In order to achieve accurate and reliable UWB TDOA-based indoor positioning, UWB measurements need to be tested in such scenarios. Currently, there exists an absence of UWB TDOA measurement identification and data collection in a cluttered environment. Furthermore, most of these datasets do not provide data collected in the presence of dynamic

Figure 4. UWB anchors and tag setup for UWB identification experiments.

obstacles. We present an Ultra-wideband Time-difference-of-arrival Indoor Localization (UTIL) dataset to fill in this gap. In this dataset, we conducted extensive UWB TDOA identification experiments under LOS and NLOS scenarios and collected multimodal sensor data from a quadrotor platform in the presence of static and dynamic obstacles. During the flight experiments, we collected raw UWB TDOA measurements with additional onboard sensor data (IMU, optical flow, and ToF laser) in four anchor constellations. Both centralized and decentralized TDOA measurements were collected under the same conditions for comparison. The combination of multimodal onboard sensors, different anchor constellations, two TDOA modalities, and diverse cluttered scenarios contained in this dataset facilitates in-depth comparisons of UWB TDOA-based quadrotor localization capabilities, a level of analysis not achievable with existing datasets. To the best of our knowledge, a comprehensive UWB TDOA dataset with *(i)* identification experiments and *(ii)* data taken in a variety of indoor environments with static and dynamic obstacles does not exist in literature.

3. UWB TDOA-based localization system

Our UWB TDOA-based localization system is sketched in Figure 1. Eight UWB anchors were pre-installed in the space with known positions. The robot equipped with an UWB tag computes the difference of the distances between the robot and the two transmitting anchors using the UWB signal arrival times. To better explain the content of our dataset, we introduce the UWB radio hardware used for data collection and provide a brief explanation of the TDOA principles.

3.1. UWB sensor

The Decawave's DWM1000 (Decaware, 2016) UWB radio sensors were used to create this dataset. The DWM1000 module is a low-cost UWB radio often used to develop cost-efficient localization solutions. The UWB TDOA measurements were collected using the Loco Positioning System (LPS) from Bitcraze, which is based on DWM1000 UWB modules (see Figure 2).

Both centralized TDOA and decentralized TDOA (Meng et al., 2016) are implemented in LPS, which are referred to as TDOA 2 and TDOA 3 by Bitcraze, respectively. In centralized TDOA systems, all the anchors are synchronized w.r.t. one master anchor and the TDOA measurements are expressed in the same clock. However, centralized TDOA systems are limited by communication constraints and suffer from single point failure (Ennasr et al., 2016). In decentralized TDOA systems, anchor pairs synchronize the timescales between each other and not with a single master anchor, which leads to scalability.

3.2. Time-difference-of-arrival principles

In this subsection, we briefly explain the TDOA principles implemented in LPS. Without loss of generality, we denote a pair of UWB anchors as anchor 1 and anchor 2. The TDOA measurement d_{12} is the difference of distances of the tag to anchors 1 and 2. The sequence of the UWB radio packets among the anchor pair and one tag is visualized in Figure 3. UWB radios, including both anchors and the tag, operate independently with their own individual clocks. These clocks are depicted as solid lines, each distinguished by a unique color. A clock synchronization process is essential for an accurate computation of TDOA measurements.

We denote the clock of anchor 1, anchor 2, and the tag as cl_1, cl_2, and cl_T in the superscripts. The transmission and the reception of a radio signal from anchor 1 are denoted as tx_1 and rx_1 in the subscripts. As an example, $t_{rx_2}^{cl_T}$ indicates the receiving timestamp of the radio packet from anchor 2 expressed in the tag's clock. UWB radio signals are transmitted with a scheduled transmission sequence. We use $\tilde{t}$ to indicate the timestamp from the previous sequence: $\tilde{t}_{tx_2}^{cl_2}$ indicates the transmitting timestamp of the radio packet from anchor 2 expressed in the clock of anchor 2 from the previous sequence. With anchor 1 and anchor 2 at positions $\boldsymbol{a}_1, \boldsymbol{a}_2 \in \mathbb{R}^3$ and one tag at position $\mathbf{p} \in \mathbb{R}^3$, the TDOA measurement between anchors 1 and 2 is computed as

$$\begin{aligned} d_{12} &= c\left[\left(t_{rx_2}^{cl_T} - t_{rx_1}^{cl_T}\right) - \alpha\left(t_{tx_2}^{cl_2} - t_{rx_1}^{cl_2} + \mathrm{tof}_{12}^{cl_2}\right)\right] \\ &= \|\mathbf{p} - \boldsymbol{a}_2\| - \|\mathbf{p} - \boldsymbol{a}_1\| \end{aligned} \tag{1}$$

where c indicates the speed of light, α is the clock correction parameter converting from anchor 2's clock to the tag's clock, $\mathrm{tof}_{12}^{cl_2}$ is the time-of-flight measurements between anchor 1 and anchor 2 expressed in anchor 2's clock, and $\|\cdot\|$ indicates the ℓ_2 norm. The clock correction parameter α is used to synchronize the clock of anchor 2 to the clock of the tag. We compute α with the timestamps from the previous sequence

$$\alpha = \frac{t_{rx_2}^{cl_T} - \tilde{t}_{rx_2}^{cl_T}}{t_{tx_2}^{cl_2} - \tilde{t}_{tx_2}^{cl_2}} \tag{2}$$

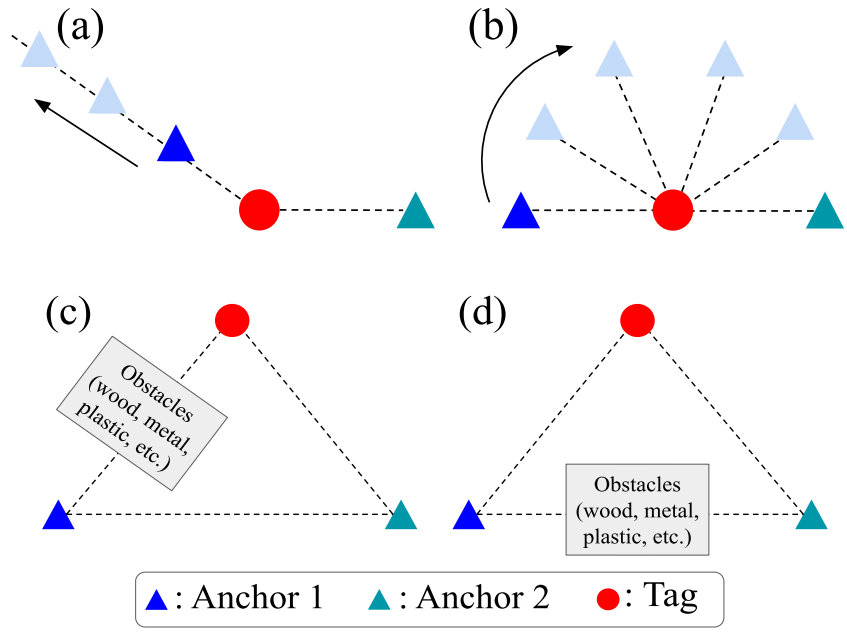

Figure 5. A diagram of the UWB identification experiments. The experiment process of LOS distance tests and LOS angle tests are illustrated in (a) and (b). The NLOS identification tests between an anchor and a tag and between two anchors are shown in (c) and (d).

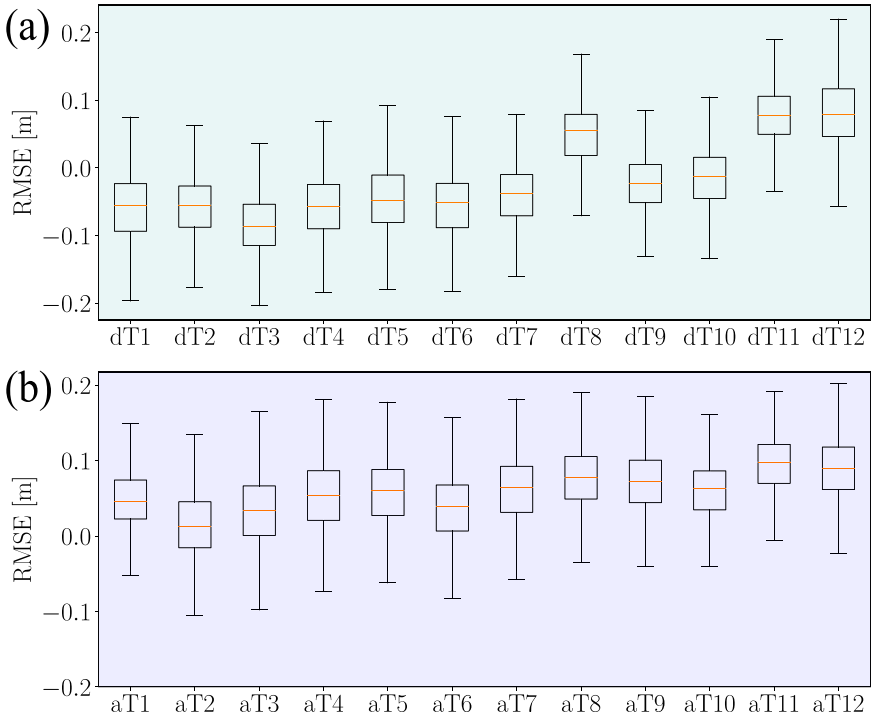

Figure 6. Measurement errors in (a) LOS distance tests (top) and (b) LOS angle tests (bottom). We indicated the distance test and angle tests as dT# and aT#, where # is the test number.

4. Data collection

4.1. Ground truth

The UTIL dataset was created at the University of Toronto Institute for Aerospace Studies (UTIAS). We collected the data in the indoor flight arena equipped with a motion capture system of 10 Vicon Vantage + cameras (Vicon, 2022). The millimeter-level accurate Vicon pose measurements were collected during UWB identification experiments and flight experiments as the ground truth measurements.

Figure 7. Obstacles used in the NLOS tests. The materials of the obstacle from left to right are cardboard, metal, wood, plastic, wood, and foam.

4.2. UWB identification dataset

In order to identify the UWB TDOA measurement performance in LOS and NLOS scenarios, we conducted a variety of LOS and NLOS experiments using two anchors and one tag. Figure 4 demonstrates the experimental setup for the identification dataset. Two UWB anchors referred to as anchor 1 and anchor 2, and one Crazyflie nano-quadrotor equipped with an UWB tag were placed on wooden structures. The ground truth pose data was provided by the motion capture system. Since only two anchors were used for the data collection, we ignored the difference between the centralized and decentralized TDOA modes and set the anchors into decentralized mode (TDOA 3). We collected the data through the Robot Operating System (ROS). Each sub-dataset was collected during a one-minute static experiment.

To assess the quality of received UWB signals, we collected the signal-to-noise ratio (SNR) and power difference (P_d) values provided in the Decawave user manual (Decawave, 2017) as the performance metrics. The computation of SNR and power difference P_d are as follows

$$\text{SNR} = \frac{\text{Am}_f}{\sigma_n}, P_d = P_r - P_f \tag{3}$$

where Am_f indicates the *First Path Amplitude value*, σ_n indicates the *Standard Deviation of Channel Impulse Response Estimate Noise* value, and P_r and P_f are the total received power and the first path power, respectively. In general, a higher SNR value or a lower P_d indicates the received radio signal is of good quality (Decawave, 2017). The four raw measurements $\{\text{Am}_f, \sigma_n, P_r, P_f\}$ can be accessed from the DW1000 UWB chip when receiving an UWB radio signal. We refer to Section 4.7 of the user manual (Decawave, 2017) for more information. Detailed data format and descriptions of the UWB identification dataset are provided in Section 5.1.

4.2.1. Line-of-sight tests. We collected UWB TDOA measurements from two LOS identification tests: *(i)* the LOS distance test and *(ii)* the LOS angle test. The data collection procedures are sketched in Figure 5(a)–(b). The positions of the tag and anchor 2 were fixed throughout the LOS data collection process. In LOS distance test, we increased the distance between anchor 1 and the tag from 0.5 m to 6.5 m in intervals of 0.5 m. In LOS angle test, we changed the angle between two anchors from 180° to 15° in intervals of 15°. The LOS TDOA measurement errors are summarized in Figure 6. We indicate the distance test and angle tests as dT# and aT#, where # is the test number.

4.2.2. Non-line-of-sight tests. In the NLOS identification tests, we fixed the positions of the tag and two anchors and placed different types of obstacles to create NLOS scenarios. Four reflective markers were placed on the top surface of the obstacle to capture both its position and dimensions during the experiments. To reflect the comprehensive performance of UWB NLOS measurements, we selected six obstacles of different types of materials commonly used in indoor settings, including cardboard, metal, wood, plastic, and foam. Figure 7 shows the obstacles we used during the experiments.

As explained in Section 3.2, the UWB tag listens to the radio packets transmitting between anchors to compute TDOA measurements. Both NLOS conditions between one anchor and the tag and between two anchors will affect TDOA measurements. Therefore, we conducted NLOS experiments under *(i)* NLOS conditions between anchor 1 and the tag and *(ii)* NLOS conditions between anchor 1 and anchor 2 (see Figure 5(c)–(d)). Considering the different radio reflection and diffraction effects with one obstacle under different orientations, we collected six sub-datasets for each NLOS condition with different orientations of the obstacle. One LOS dataset was collected for comparison. We present one NLOS identification experiment and summarize the measurement errors induced by metal occlusions in Figure 8 as an example.

4.3. Flight dataset

The flight dataset is a comprehensive multimodal collection from a customized quadrotor platform in a range of cluttered indoor environments, featuring both static and dynamic obstacles.

4.3.1. Indoor flight arena. We collected the UWB TDOA flight dataset in the indoor flight arena measuring approximately 7.0 m × 8.0 m × 3.5 m. Printed AprilTags (Olson, 2011) were attached to the soft mattresses to provide visual features for optical flow. Figure 9 is a photograph of our flight arena during data collection.

To ensure the accuracy of our dataset, we performed anchor surveying for each of our data collection sessions, leading to four different anchor constellations. In each anchor constellation, eight UWB anchors were pre-installed in the flight arena. We refer to the Vicon frame as the inertial frame $\mathcal{F}_\mathcal{I}$ and the anchor frame as $\mathcal{F}_\mathcal{A}$ (see Figure 9). To maximize the utilization of the indoor environment, we placed the UWB anchors along the boundary of the space to construct the anchor constellations, resulting in their positions outside the field of view of the Vicon system.

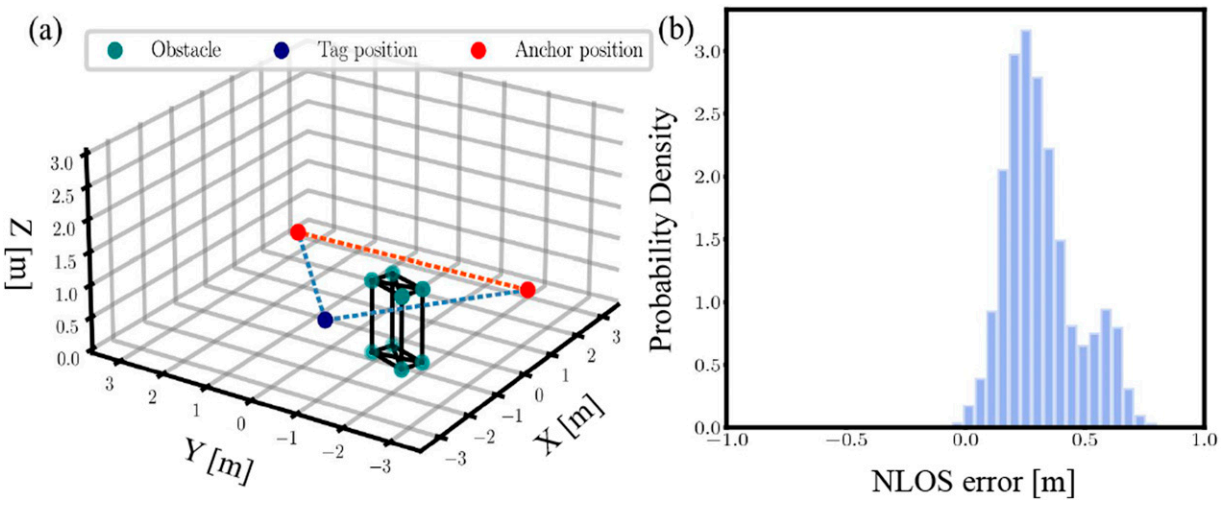

Figure 8. One example of NLOS identification experiments is shown in (a). A histogram of measurement errors induced by placing the metal obstacle between one anchor and the tag is summarized in (b).

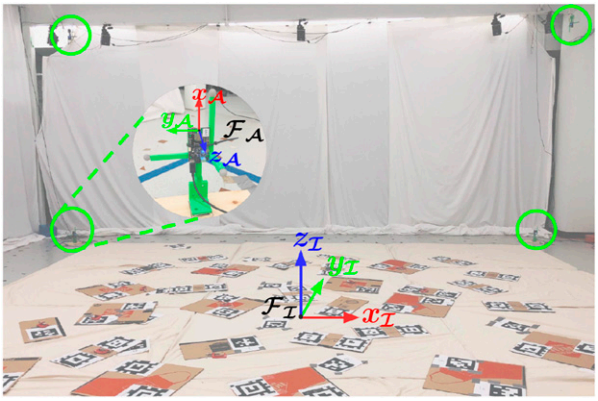

Figure 9. A photo of the flight arena. The UWB anchors are enclosed with green circles. The inertial frame and UWB anchor frame are indicated as $\mathcal{F}_{\mathcal{I}}$ and $\mathcal{F}_{\mathcal{A}}$, respectively. The ground is covered with soft mattresses with a thickness of two inches (5.08 cm). Printed AprilTags are attached to the mattresses to provide visual features for the optical flow.

Consequently, we used a millimeter-accurate Leica total station (Leica, 2021) for the anchor survey process and transformed the survey results back into the Vicon inertial frame subsequently for use. To align the total station frame and the inertial frame, we used the total station to survey six reflective markers with known positions in the inertial frame and compute the transformation matrix by aligning the point-clouds (Besl and McKay, 1992). To assess the quality of the frame alignment between the total station frame and the inertial frame, we computed the reprojection error of the six reflective markers. The survey points in the total station frame were converted into the inertial frame with a root-mean-squared error (RMSE) of around 1.12 mm. Since the low-cost DWM1000 UWB chip is reported to have pose-related measurement biases (Zhao et al., 2021; Ledergerber and D'Andrea, 2017), we intended to survey both the position and the orientation of each anchor for reproducibility.

During the anchor surveying process, we surveyed the UWB antenna center together with three reflective markers on the extended arms of each anchor stand (see Figure 9). The positions of these markers in the anchor frame were pre-measured. Then we leveraged the surveyed marker positions, converted into the inertial frame, along with their known positions in the anchor frame to compute the pose (position and orientation) of each anchor through point-cloud alignment (Besl and McKay, 1992). We provide both Python (`anchor_survey.py`) and MATLAB (`anchor_survey.m`) scripts in our development kit for the users to replicate this process.

4.3.2. Quadrotor platform. We built a customized quadrotor based on the Crazyflie Bolt flight controller (Bitcraze, 2022) with an inertial measurement unit (IMU) and attached commercially available extension boards (so-called decks) from Bitcraze for data collection (see Figure 10). The LPS UWB tag was mounted vertically on the top since the DWM1000 antenna radiation pattern is uniform in its azimuth plane (Decaware, 2016). A flow deck attached at the bottom provides optical flow measurements, and a laser-based time-of-flight (ToF) sensor provides the local altitude information. The accelerometer and gyroscope data were obtained from the onboard IMU. A micro SD card deck was used to log the raw sensor data received by the flight control board with high-precision microsecond timestamps. The customized quadrotor communicates with a ground station computer over a 2.4 GHz USB radio dongle (Crazyradio PA) for high-level interaction. In terms of software, we used the Crazyswarm package (Preiss et al., 2017) to send high-level commands, such as takeoff/landing and start/stop of data logging, and pre-defined waypoints. The pose of the quadrotor measured by the motion capture system was also sent to the quadrotor as an external measurement for the onboard state estimation.

4.3.3. Calibration and latency. We refer to the offset between the center of a sensor and the center of vehicle frame $\mathcal{F}_\mathcal{V}$ as sensor extrinsic parameters. We calibrated the sensor extrinsic parameters by manually measuring the translation vectors from the vehicle center to onboard sensors (UWB tag and flow deck). The IMU was assumed to be aligned with the vehicle center. The translation vector from the vehicle to the UWB tag was measured as $r_{uv} = [-0.012, 0.001, 0.091]^T$ m and the measurement model is

$$d_{ij} = \left\|(\mathbf{C}_{\mathcal{IV}} r_{uv} + \mathbf{p}) - \boldsymbol{a}_j\right\| - \left\|(\mathbf{C}_{\mathcal{IV}} r_{uv} + \mathbf{p}) - \boldsymbol{a}_i\right\| \quad (4)$$

where $\mathbf{C}_{\mathcal{IV}}$ is the rotation matrix from the vehicle frame $\mathcal{F}_\mathcal{V}$ to the inertial frame $\mathcal{F}_\mathcal{I}$ and $\mathbf{p}$ indicates the position of the vehicle expressed in the inertial frame.

Similarly, the translation vector from the vehicle to the flow-deck extension board was measured to be $r_{fv} = [0.000, 0.000, -0.012]^T$ m. Since we covered the ground of the flight arena with 2-inch thick (0.0508 m) mattresses for protection during data collection, the thickness of the mattress needs to be taken into account while using the ToF measurements. We refer to Section 6.5 of Greiff (2017) for detailed information on the flow-deck extension board.

Given our adoption of the same software and hardware configuration as the Crazyswarm project (Preiss et al., 2017)

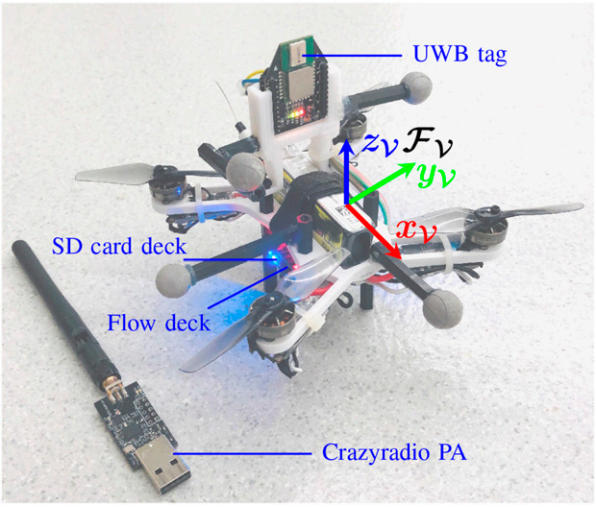

Figure 10. The customized quadrotor platform based on the Crazyflie Bolt flight controller.

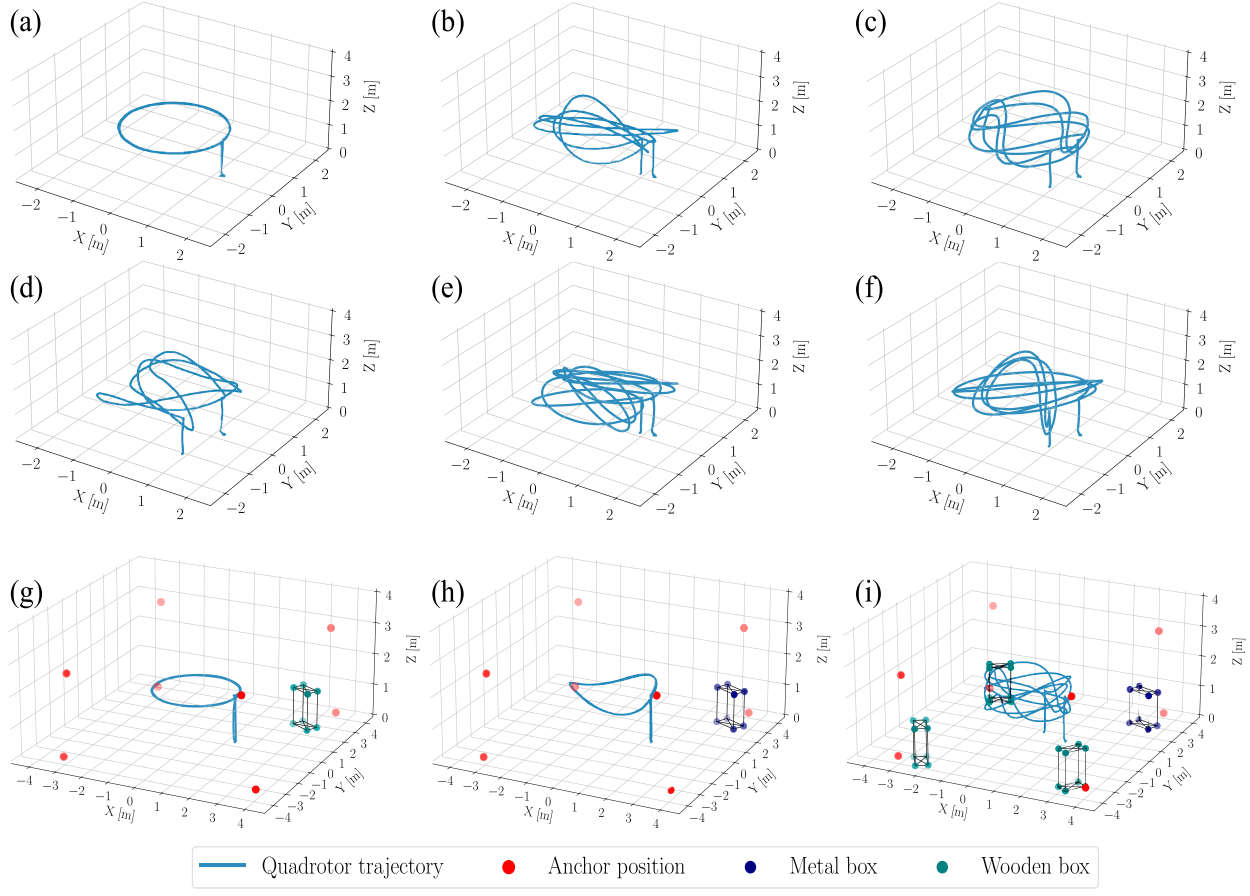

Figure 11. Flight trajectories and static NLOS conditions in the flight dataset. The six flight trajectories in constellation #1, #2, and #3 are shown in (a)–(f). Note that the trajectories in constellation #1 have a smaller separation in the x and y axes due to the smaller constellation coverage. The three static NLOS conditions and the anchor positions in constellation #4 together with the three flight trajectories are shown in (g)–(i).

Table 2. Format of the `.csv` files in each static sub-dataset.

CSV Column	Value	Description
1	d_{12} [m]	TDOA measurements $d_{12} = d_2 - d_1$
2	d_{21} [m]	TDOA measurements $d_{21} = d_1 - d_2$
3	SNR_1	SNR value of the UWB radio packet sent from anchor 1 received by the tag
4	P_{d1} [dB]	Power difference value of the UWB radio packet sent from anchor 1 received by the tag
5	SNR_2	SNR value of the UWB radio packet sent from anchor 2 received by the tag
6	P_{d2} [dB]	Power difference value of the UWB radio packet sent from anchor 2 received by the tag
7	SNR^{an1}	SNR value of the UWB radio packet sent from anchor 2 received by anchor 1
8	P_d^{an1} [dB]	Power difference value of the UWB radio packet sent from anchor 2 received by anchor 1
9	r_{12}^{cl1} [m]	Distance between anchors 1 and 2 computed by tof_{12}^{cl1}
10	SNR^{an2}	SNR value of the UWB radio packet sent from anchor 1 received by anchor 2
11	P_d^{an2} [dB]	Power difference value of the UWB radio packet sent from anchor 1 received by anchor 2
12	r_{12}^{cl2} [m]	Distance between anchors 1 and 2 computed by tof_{12}^{cl2}

Table 3. Summary of the CSV flight dataset format.

CSV column	Name	Format
1 ~ 4	UWB TDOA	(timestamp [ms], Anchor-ID i, Anchor-ID j, d_{ij} [m])
5 ~ 8	Acceleration	(timestamp [ms], acc. x [G], acc. y [G], acc. z [G])
9 ~ 12	Gyroscope	(timestamp [ms], gyro. x [deg/s], gyro. y[deg/s], gyro. z[deg/s])
13 ~ 14	ToF laser-ranging	(timestamp [ms], ToF [m])
15 ~ 17	Optical flow	(timestamp [ms], dpixel x, dpixel y)
18 ~ 19	Barometer	(timestamp [ms], barometer [asl])
20 ~ 27	Ground truth pose	(timestamp [ms], x [m], y[m], z[m], q_x, q_y, q_z, q_w)

for our flight experiments, we direct readers to Section XI-A of Preiss et al. (2017) for a comprehensive explanation of the latency measurement process, in which the reported latency for a single vehicle is approximately 11 ms.

4.3.4. Data collection process. We operated the motion capture system at a fixed sample frequency of 200 Hz and sent the measured quadrotor pose to the onboard error-state Kalman filter with a small standard deviation, 0.001 m for position and 0.05 rad for orientation, for state estimation. Onboard the quadrotor, the raw UWB TDOA measurements, gyroscope, accelerometer, optical flow, ToF laser-ranging, barometer, and the Vicon pose measurements (sent from the ground station) were recorded as event streams. We treat the Vicon pose measurements logged onboard as the ground truth data. Each datapoint was timestamped with the onboard microsecond timer, and the resulting time series were written to the micro SD card as a binary file. Python scripts are provided to parse and analyze the binary data.

During the data collection process, we commanded the quadrotor to fly six different trajectories in constellation #1, #2, and #3 under LOS conditions. The six flight trajectories are summarized in Figure 11(a)–(f). In constellation #4, we created three cluttered environments with static obstacles (see Figure 11(g)–(i)) and two cluttered environments with one dynamic metal obstacle. During the dynamic obstacle experiment, we moved the metal cabinet manually and intentionally blocked two anchors temporarily during the flights. Note that the human body also acted as a dynamic obstacle in these cases. The onboard sensor data was collected over three different trajectories. In each experiment, we commanded the quadrotor to fly the same trajectories with both centralized and decentralized TDOA modes for comparison. For the flight experiments with dynamic obstacles, we created animations in `scripts/flight-dataset/animations` folder to demonstrate the data collection process. We also conducted a couple of manual data collection experiments with a human body involved in constellations #3 and #4.

5. Data format

5.1. UWB identification data format

The UWB identification dataset consists of data collected from *(i)* LOS distance and angle tests and *(ii)* NLOS identification experiments with different types of obstacles. In each sub-dataset, we provide a `.csv` file containing the collected data and a `.txt` file containing the poses of the tag and two anchors in one folder. For NLOS identification experiments, the positions of the four markers on the obstacles are also included in the `.txt` file. The format of the `.csv` file and brief descriptions of each value are summarized in Table 2. The format of the position data provided in the `.txt` file is (x, y, z) in meters. The orientation is provided as a unit quaternion (q_x, q_y, q_z, q_w), where q_w and (q_x, q_y, q_z) are the scalar and the vector components, respectively.

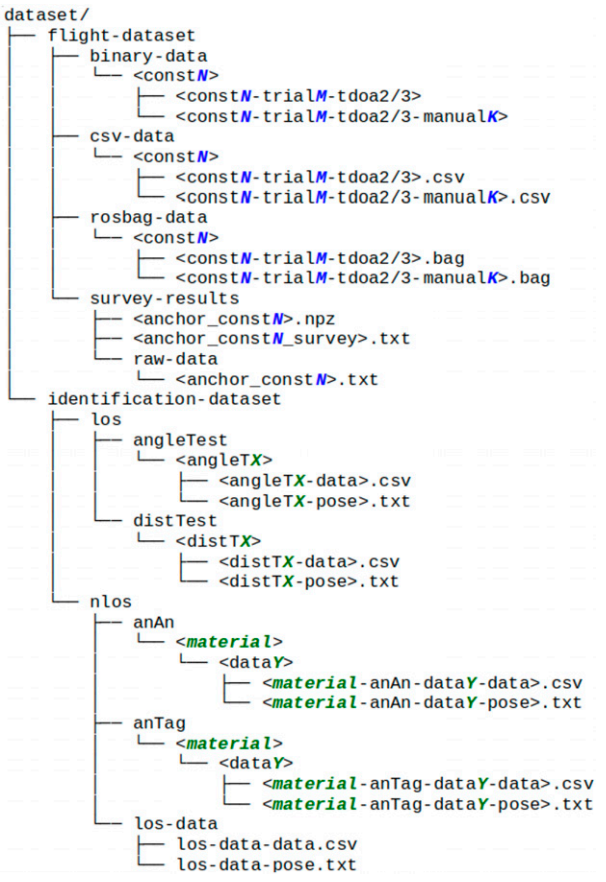

Figure 12. The file structure and naming convention of the UTIL dataset. In the flight dataset, we summarized the binary, CSV, and rosbag data according to different anchor constellations. In the identification dataset, we separate the LOS and NLOS testing data with each NLOS dataset containing the material of the obstacle in the filename.

5.2. Flight experiment data format

The flight experiment data were collected onboard the quadrotor during the flights as binary files. We provide the converted CSV and rosbag data and the corresponding Python scripts used for data parsing. For each UWB constellation, we provide the raw Leica total station survey results and computed anchor poses in `.txt` files. In each sub-dataset, we provide the timestamped accelerometer, gyroscope, UWB TDOA, optical flow, ToF laser-ranger, barometer measurements, and the ground truth measurements of the quadrotor's pose during the flight. The CSV data format for each sensor data is summarized in Table 3. The detailed file structure and naming convention are shown in Figure 12.

6. Development kit and benchmark

As part of this dataset, we provide a development kit with both Python and MATLAB scripts for the users to parse the data. For the UWB identification dataset, we provide scripts to visualize the distribution of the collected data. For the flight dataset, we provide a range of different ways to visualize the sensor data and the data collection process. We also provide the STL files for the 3D printed quadrotor frame and the UWB tag support in the `setup_files/stl-files` folder. Finally, an error-state Kalman filter (ESKF) implementation is provided for users to evaluate the

Table 4. Root-mean-square errors in meters obtained from benchmark on all sequences of the UTIL dataset using IMU and UWB TDOA measurements. This evaluation is conducted using an error-state Kalman filter and a batch estimation algorithm, with lower error values highlighted in bold format. We indicate the constellation as `Const.` for short. The data sequences indicate the number of `trial#` in `Const.`#1 ∼ #3 and `trial#.traj#` in `Const.`#4, where `m#` indicates a trial of data collected manually.

		TDOA2		TDOA3	
Data Seq.		ESKF	Batch	ESKF	Batch
Const. 1	1	0.108	**0.097**	0.144	**0.099**
	2	0.122	**0.107**	0.144	**0.104**
	3	0.109	**0.097**	0.123	**0.095**
	4	0.111	**0.099**	0.127	**0.093**
	5	0.115	**0.106**	0.149	**0.120**
	6	0.123	**0.107**	0.135	**0.103**
Const. 2	1	0.103	**0.098**	0.114	**0.082**
	2	0.114	**0.096**	0.116	**0.078**
	3	**0.108**	0.109	0.117	**0.079**
	4	0.094	**0.081**	0.121	**0.074**
	5	0.122	**0.099**	0.125	**0.076**
	6	0.106	**0.094**	0.117	**0.097**
Const. 3	1	0.245	**0.127**	0.232	**0.144**
	2	0.194	**0.100**	0.225	**0.116**
	3	0.189	**0.093**	0.214	**0.124**
	4	0.215	**0.116**	0.204	**0.114**
	5	0.220	**0.117**	0.241	**0.126**
	6	0.193	**0.085**	0.211	**0.099**
	m1	0.265	**0.159**	N/A	N/A
	m2	0.335	**0.196**	N/A	N/A
	m3	N/A	N/A	0.340	**0.204**
	m4	N/A	N/A	0.355	**0.182**
Const. 4	1.1	0.201	**0.176**	0.207	**0.146**
	1.2	0.168	**0.135**	0.163	**0.117**
	1.3	0.194	**0.146**	0.190	**0.139**
	2.1	0.231	**0.202**	0.221	**0.164**
	2.2	0.200	**0.158**	0.219	**0.170**
	2.3	0.222	**0.185**	0.238	**0.177**
	3.1	0.919	**0.788**	0.742	**0.563**
	3.2	0.718	**0.624**	0.558	**0.482**
	3.3	0.651	**0.571**	0.674	**0.529**
	4.1	0.818	**0.704**	0.759	**0.612**
	4.2	0.766	**0.648**	0.845	**0.669**
	4.3	0.735	**0.636**	0.838	**0.669**
	5.1	0.473	**0.397**	0.432	**0.334**
	5.2	0.470	**0.397**	0.435	**0.312**
	5.3	0.395	**0.340**	0.443	**0.325**
	6.1	0.509	**0.434**	0.623	**0.486**
	6.2	0.459	**0.370**	0.618	**0.458**
	6.3	0.517	**0.451**	0.578	**0.487**
	m1	0.529	**0.519**	N/A	N/A
	m2	**0.587**	0.613	N/A	N/A
	m3	0.333	**0.266**	N/A	N/A

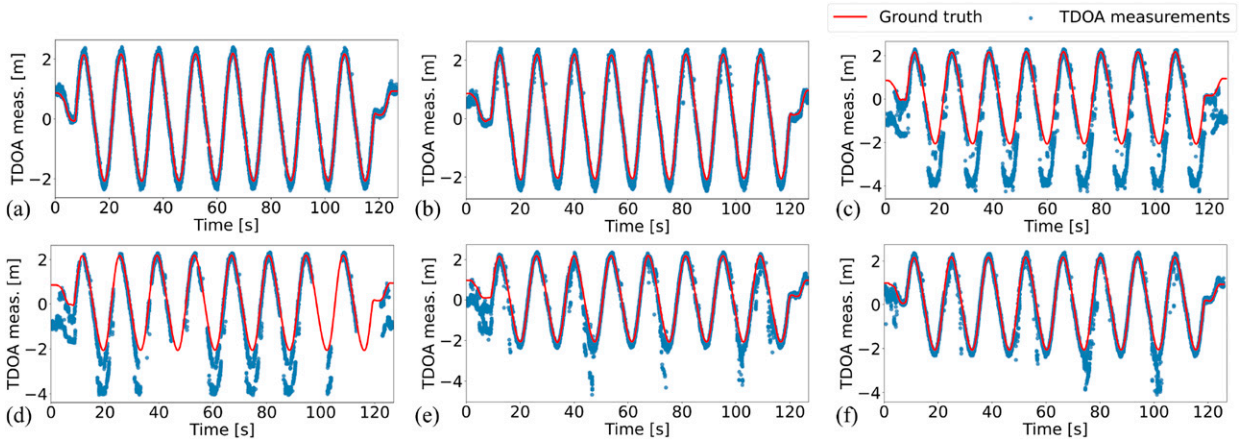

Figure 13. The UWB TDOA measurement d_{23} collected from the same circle trajectory in constellation #4 under different LOS/NLOS conditions. The measurements under clear LOS conditions are shown in (a). In static NLOS conditions induced by (b) one wooden obstacle, (c) one metal obstacle, and (d) one metal and three wooden obstacles, we can observe consistent measurement biases over repeated trajectories. In dynamic NLOS conditions caused by (e) one metal obstacle and (f) one metal obstacle and three wooden obstacles, the induced measurement errors are less predictable.

UWB TDOA-based positioning performance in different scenarios. The development kit and instructions can be found at https://utiasdsl.github.io/util-uwb-dataset/.

We provide a localization performance benchmark of the proposed dataset using IMU and UWB TDOA measurements. This evaluation is conducted with an error-state Kalman filter (ESKF) (Goudar and Schoellig, 2021) and a batch estimation algorithm (Barfoot, 2017). A chi-square test outlier rejection mechanism is applied in the ESKF to discard large outliers. The root-mean-square error (RMSE) in meters is summarized in Table 4. The benchmark results reveal that ESKF and batch estimation demonstrates commendable performance with an approximate positioning error of 10 cm in obstacle-free environments (constellations #1, #2, and #3). However, in constellation #4, the positioning performance of conventional estimation algorithms deteriorates greatly, primarily due to obstacle-induced measurement errors. These findings highlight substantial opportunities for researchers to develop novel estimation algorithms and enhance localization performance in cluttered indoor environments.

7. Dataset usage

In this section, we provide two potential usages of this dataset for users followed by a discussion of potential research directions.

7.1. UWB TDOA measurement modeling

For UWB TDOA localization, modeling the measurement errors under LOS and NLOS scenarios is important for the design of localization algorithms (Prorok et al., 2012; Ruiz and Granja, 2017). The stationary UWB TDOA signal testing data can be used to model the distribution of the UWB TDOA measurement errors under various LOS and NLOS conditions. One example of using the identification dataset to model UWB TDOA measurement error modeling can be found in Zhao et al. (2022).

7.2. Accurate UWB TDOA-based localization

The flight dataset can be used to develop UWB TDOA-based localization algorithms. We provide the UWB measurements under centralized TDOA mode (TDOA2) and decentralized TDOA mode (TDOA3). The flight dataset collected in constellations 1 and 2 can be used to compare the localization performance between different UWB modes using low-cost DWM1000 UWB modules.

It is reported in the literature that the low-cost DW1000 UWB chips suffer from systematic measurement biases (Zhao et al., 2021; Ledergerber and D'Andrea, 2017). Also, the UWB radio measurements are often corrupted with multi-path and NLOS signal propagation in real-world scenarios. In cluttered indoor environments, multi-path and NLOS radio propagation cannot be avoided in general. We summarized the UWB TDOA measurement d_{23} in constellation #4 in different LOS/NLOS scenarios in Figure 13. The quadrotor was commanded to execute the same and repeated circle trajectory. We can observe in Figure 13(b)–(d) that static obstacles consistently influence the UWB measurements. Also, UWB measurements can be completely blocked due to severe NLOS conditions. However, in dynamic NLOS scenarios (see Figure 13(e) and (f)), the induced measurement errors do not remain consistent. Hence, the flight dataset collected in constellation #4 can be used to design new algorithms to cope with UWB measurement errors and noise so as to achieve robust and accurate UWB-based positioning performance in such challenging and highly dynamic environments.

In the past decade, researchers have dedicated efforts to enhance UWB TDOA localization performance while keeping costs low through the use of economical hardware. Despite these efforts, non-line-of-sight (NLOS) and multi-path radio propagation remain the major factors hindering the localization performance of UWB-based systems. Identifying the measurement outliers and systematically handling the biased and non-Gaussian noise distributions (Huang et al., 2022; Zhao et al., 2023) in cluttered environments remains to be promising research directions. Additionally, the exploration of continuous-time estimation techniques (Goudar et al., 2023; Li et al., 2023) emerges as another promising research direction for asynchronous UWB-inertial localization systems. Furthermore, it is necessary to conduct observability analysis (Goudar and Schoellig, 2021) on system states and properly address the unobserved states to achieve consistent estimation (Lisus et al., 2023).

8. Conclusion

In this paper, we present the UTIL dataset, a comprehensive UWB TDOA dataset based on the low-cost DWM1000 UWB modules. Our dataset consists of *(i)* an UWB identification dataset under various LOS and NLOS conditions and *(ii)* a multimodal flight dataset collected with a cumulative total of around 150 min of real-world flights in cluttered indoor environments with four anchor constellations. Obstacles of different types of materials commonly used in indoor settings, including cardboard, metal, wood, plastic, and foam, were used to create NLOS scenarios. During the flights, we collected raw UWB TDOA measurements with additional onboard sensor data (IMU, optical flow, and ToF laser) and millimeter-accurate ground truth data from a motion capture system onboard a quadrotor platform. The combination of multimodal onboard sensors, different anchor constellations, two TDOA modalities, and diverse cluttered scenarios contained in this dataset facilitates in-depth comparisons of UWB TDOA-based quadrotor localization capabilities. We hope this dataset can foster research in improving the UWB TDOA-based positioning performance in cluttered indoor environments.

Acknowledgements

We would like to thank Kristoffer Richardsson and Tobias Antonsson (Bitcraze) for their guidance on the software and hardware development of the customized quadrotor platform. This work was supported in part by the Natural Sciences and Engineering Research Council of Canada (NSERC) and in part by the Canada CIFAR AI Chairs Program.

Declaration of conflicting interests

The author(s) declared no potential conflicts of interest with respect to the research, authorship, and/or publication of this article.

Funding

The author(s) received no financial support for the research, authorship, and/or publication of this article.

ORCID iDs

Wenda Zhao https://orcid.org/0000-0002-4288-0582
Abhishek Goudar https://orcid.org/0000-0002-4438-5876
Angela P. Schoellig https://orcid.org/0000-0003-4012-4668

References

Adidas (2022) Adidas reveals the first FIFA world cup official match ball featureing connected ball technology. URL https://news.adidas.com/football/adidas-reveals-the-first-fifa-world-cup–official-match-ball-featuring-connected-ball-technology/s/cccb7187-a67c-4166-b57d-2b28f1d36fa0

Ahmed S, Wang D, Park J, et al. (2021) UWB-gestures, a public dataset of dynamic hand gestures acquired using impulse radar sensors. *Scientific Data* 8(1): 102–109.

Apple (2022) Nearby interaction with UWB. URL https://developer.apple.com/nearby-interaction/.

Arjmandi Z, Kang J, Park K, et al. (2020) Benchmark dataset of ultra-wideband radio based UAV positioning. In: 2020 IEEE 23rd international conference on intelligent transportation systems (ITSC). Rhodes, Greece, 20–23 September 2020, pp. 1–8. IEEE.

Barfoot TD (2017) *State Estimation for Robotics*. Cambridge, UK: Cambridge University Press.

Barral V, Escudero CJ, García-Naya JA, et al. (2019a) NLOS identification and mitigation using low-cost UWB devices. *Sensors* 19(16): 3464.

Barral V, Suárez-Casal P, Escudero CJ, et al. (2019b) Multi-sensor accurate forklift location and tracking simulation in industrial indoor environments. *Electronics* 8(10): 1152.

Besl PJ and McKay ND (1992) Method for registration of 3-D shapes. *Sensor fusion IV: Control Paradigms and Data Structures* 1611: 586–606.

Bitcraze (2022) Bitcraze Crazyflie Bolt flight controller. URL https://www.bitcraze.io/products/crazyflie-bolt-1-1/.

Bocus MJ and Piechocki R (2022) A comprehensive ultra-wideband dataset for non-cooperative contextual sensing. *Scientific Data* 9(1): 650.

Bregar K and Mohorčič M (2018) Improving indoor localization using convolutional neural networks on computationally restricted devices. *IEEE Access* 6: 17429–17441.

Brishtel I, Krauss S, Chamseddine M, et al. (2023) Driving activity recognition using UWB radar and deep neural networks. *Sensors* 23(2): 818.

Decaware (2016) Decawave DW1000 datasheet. URL https://www.decawave.com/wp-content/uploads/2020/09/DWM1000-Datasheet.pdf.

Decawave (2017) Decawave DW1000 user manual. URL https://www.decawave.com/sites/default/files/resources/dw1000_user_manual_2.11.pdf.

Delamare M, Duval F and Boutteau R (2020) A new dataset of people flow in an industrial site with UWB and motion capture systems. *Sensors* 20(16): 4511.

Dowsett B (2022) The world cup's new high-tech ball will change soccer forever. URL https://fivethirtyeight.com/features/the-world-cups-new-high-tech-ball-will-change-soccer-forever/.

Enge PK (1994) The global positioning system: signals, measurements, and performance. *International Journal of Wireless Information Networks* 1(2): 83–105.

Ennasr O, Xing G and Tan X (2016) Distributed time-difference-of-arrival (TDOA)-based localization of a moving target. In: 2016 IEEE 55th conference on decision and control (CDC), Las Vegas, NV, USA, 12–14 December 2016, pp. 2652–2658. IEEE.

Fontaine J, Shahid A and Van Herbruggen B (2023) *Industrial UWB Localization Dataset Containing Channel Impulse Response Data* URL. DOI: 10.21227/w0v9-5e35.

Ge Y, Tang C, Li H, et al. (2023) A large-scale multimodal dataset of human speech recognition. *arXiv preprint arXiv: 2303.08295*.

Goudar A and Schoellig AP (2021) Online spatio-temporal calibration of tightly-coupled ultrawideband-aided inertial localization. In: 2021 IEEE/RSJ International Conference on Intelligent Robots and Systems (IROS), Prague, Czech Republic, 27 September 2021–01 October 2021, pp. 1161–1168. IEEE.

Goudar A, Barfoot TD and Schoellig AP (2023) Continuous-time range-only pose estimation. arXiv preprint arXiv:2304.09043.

Greiff M (2017) *Modelling and Control of the Crazyflie Quadrotor for Aggressive and Autonomous Flight by Optical Flow Driven State Estimation*. Master's Thesis. Lund, Sweden: Lund University.

Hamer M and D'Andrea R (2018) Self-calibrating ultra-wideband network supporting multi-robot localization. *IEEE Access* 6: 22292–22304.

Huang Q, Pu C, Khosoussi K, et al. (2022) Incremental non-gaussian inference for SLAM using normalizing flows. *IEEE Transactions on Robotics* 39(2): 1458–1475.

KINEXON (2022) Capture and analyze the ball's position and inertial data in real-time. URL https://kinexon.com/technology/ball-tracking/#ballsensor.

Ledergerber A and D'Andrea R (2017) Ultra-wideband range measurement model with Gaussian processes. In: Proceedings of the IEEE conference on control technology and applications (CCTA), Maui, HI, USA, 27–30 August 2017, pp. 1929–1934.

Ledergerber A and D'Andrea R (2019) Ultra-wideband angle of arrival estimation based on angle-dependent antenna transfer function. *Sensors* 19(20): 4466.

Leica G (2021) Leica geosystems robotic total station. URL https://leica-geosystems.com/products/total-stations/robotic-total-stations

Li J, Bi Y, Li K, et al. (2018) Accurate 3d localization for MAV swarms by UWB and IMU fusion. In: 2018 IEEE 14th International Conference on Control and Automation (ICCA), Anchorage, AK, USA, 12–15 June 2018, pp. 100–105. IEEE.

Li K, Cao Z and Hanebeck UD (2023) Continuous-time ultra-wideband-inertial fusion. *IEEE Robotics and Automation Letters* 8: 4338–4345.

Lisus D, Cohen M and Forbes JR (2023) Know what you don't know: consistency in sliding window filtering with unobservable states applied to visual-inertial slam. *IEEE Robotics and Automation Letters* 8: 3382–3389.

Meng W, Xie L and Xiao W (2016) Optimal TDOA sensor-pair placement with uncertainty in source location. *IEEE Transactions on Vehicular Technology* 65(11): 9260–9271.

Morón PT, Salimpour S, Fu L, et al. (2023) Benchmarking UWB-based infrastructure-free positioning and multi-robot relative localization: dataset and characterization. arXiv preprint arXiv:2305.08532.

Nguyen TH, Nguyen TM and Xie L (2021a) Range-focused fusion of camera-IMU-UWB for accurate and drift-reduced localization. *IEEE Robotics and Automation Letters* 6(2): 1678–1685.

Nguyen TM, Yuan S, Cao M, et al. (2021b) NTU VIRAL: a visual-inertial-ranging-lidar dataset, from an aerial vehicle viewpoint. *The International Journal of Robotics Research* 41(3): 02783649211052312.

Olson E (2011) AprilTag: a robust and flexible visual fiducial system. In: 2011 IEEE international conference on robotics and automation, Shanghai, China, 09–13 May 2011, pp. 3400–3407. IEEE.

Pfeiffer S, Wagter C and Croon GC (2021) A computationally efficient moving horizon estimator for ultra-wideband localization on small quadrotors. *IEEE Robotics and Automation Letters* 6(4): 6725–6732.

Preiss JA, Honig W, Sukhatme GS, et al. (2017) Crazyswarm: a large nano-quadcopter swarm. In: 2017 IEEE international conference on robotics and automation (ICRA), Singapore, 29 May 2017–03 June 2017, pp. 3299–3304. IEEE.

Prorok A, Gonon L and Martinoli A (2012) Online model estimation of ultra-wideband TDOA measurements for mobile robot localization. In: 2012 IEEE international conference on robotics and automation, Saint Paul, MN, USA, 14–18 May 2012, pp. 807–814. IEEE.

Qorvo (2022) Qorvo UWB solutions certified for Apple U1 interoperability. URL https://www.qorvo.com/newsroom/news/2022/qorvo-uwb-solutions-certified-for-apple-u1-interoperability.

Queralta JP, Almansa CM, Schiano F, et al. (2020) UWB-based system for UAV localization in GNSS-denied environments: characterization and dataset. In: 2020 IEEE/RSJ international conference on intelligent robots and systems (IROS), Las Vegas, NV, USA, 24 October 2020–24 January 2021, pp. 4521–4528. IEEE.

Raza U, Khan A, Kou R, et al. (2019) Dataset: indoor localization with narrow-band, ultra-wideband, and motion capture systems. In: Proceedings of the 2nd workshop on data acquisition to analysis, New York, USA, 10 November, pp. 34–36.

Robert Triggs CW (2022) What is UWB, and why is it in my phone? Ultra-wideband technology, explained. URL https://www.androidauthority.com/what-is-uwb-1151744/.

Jimenez Ruiz AR and Seco Granja F (2017) Comparing ubisense, bespoon, and Decawave UWB location systems: indoor performance analysis. *IEEE Transactions on Instrumentation and Measurement* 66(8): 2106–2117.

TDSR (2022) TDSR P440 time domain UWB module. URL https://tdsr-uwb.com/products-p440-uwb-module/.

Vicon MCS (2022) Vicon Vantage+ cameras. URL https://www.vicon.com/hardware/cameras/vantage/.

Vleugels R, Van Herbruggen B, Fontaine J, et al. (2021) Ultra-wideband indoor positioning and IMU-based activity recognition for ice hockey analytics. *Sensors* 21(14): 4650.

Zafari F, Gkelias A and Leung KK (2019) A survey of indoor localization systems and technologies. *IEEE Communications Surveys & Tutorials* 21(3): 2568–2599.

Zhang J, Qi Q, Cheng H, et al. (2023) A multi-target localization and vital sign detection method using ultra-wide band radar. *Sensors* 23(13): 5779.

Zhao W, Panerati J and Schoellig AP (2021) Learning-based bias correction for time difference of arrival ultra-wideband localization of resource-constrained mobile robots. *IEEE Robotics and Automation Letters* 6(2): 3639–3646.

Zhao W, Goudar A and Schoellig AP (2022) Finding the right place: sensor placement for UWB time difference of arrival localization in cluttered indoor environments. *IEEE Robotics and Automation Letters* 7: 6075–6082.

Zhao W, Goudar A, Tang M, et al. (2023) Uncertainty-aware gaussian mixture model for UWB time difference of arrival localization in cluttered environments. In: 2023 IEEE/RSJ international conference on intelligent robots and systems (IROS), Detroit, Michigan, USA, 1-5 October, pp. 5266–5273. IEEE.

Zhengliang Z, Degui Y, Junchao Z, et al. (2021) Dataset of human motion status using IR-UWB through-wall radar. *Journal of Systems Engineering and Electronics* 32(5): 1083–1096.